Influence of the Length of a Photovoltaic Single-Axis Tracker Mounting Rail

J.H. Koekemoer[a], J.R. Bredell[b], G. Venter[c], J. Reinecke[d]

Received 19 February 2024, in revised form 4 October 2024 and accepted 1 November 2024

Abstract: ***Single-axis trackers are actuated structures in utility-scale photovoltaic power plants. Wind loads on trackers often govern their structural design. A critical tracker component is the mounting rail, which forms the structural support between the rotating horizontal torque tube and the photovoltaic modules. The rails are thin gauge cold-formed steel members with bolted connections. Recent design trends show decreasing mounting rail length to reduce cost. This study investigated the influence of rail length in a one-in-portrait tracker using linear static finite element analyses. The finite element models of photovoltaic modules were calibrated using experimental force-displacement data. A single glass layer of the full laminate thickness required a calibrated Young's modulus of 56.5 GPa compared to 70 GPa nominally. The investigated rail lengths ranged between 900 mm and 400 mm and support bifacial photovoltaic modules with dimensions 2037 mm $\times$ 1055 mm. With the 900 mm length used as the reference case, it was shown that stresses in the photovoltaic module frame due to simplified wind loads increased by up to 124 % as the rail lengths were reduced. Stresses in the solar glass and crystalline silicon cells increased by as much as 65 %. Uniform and non-uniform distributed loads were considered. Significantly higher stresses were seen for non-uniform loads with a centre of pressure eccentric to the torque tube, which more accurately represents wind loads according to design codes and field measurements. A uniform distributed load, typically used for dynamic load qualification testing on photovoltaic modules, is inadequate for calculating mounting rail deformations and stresses expected from wind loads.***

Additional keywords: Photovoltaic, solar energy, single-axis tracker, finite element analysis, wind loads

Nomenclature

Roman

L_R	Rail length [m]

[a] Member. Department of Mechanical and Mechatronic Engineering, Stellenbosch University, South Africa. E-mail: hanneskoekemoer08@gmail.com

[b] Member. Department of Mechanical and Mechatronic Engineering, Stellenbosch University, South Africa. E-mail: jrbredell@sun.ac.za

[c] Member. Department of Mechanical and Mechatronic Engineering, Stellenbosch University, South Africa. E-mail: gventer@sun.ac.za

[d] Member. Scatec Africa (Pty) Ltd, Cape Town, South Africa. E-mail: Josh.Reinecke@scatec.com

Greek

σ_1	Maximum principal stress [MPa]
σ_{VM}	Von Mises stress [MPa]

1 Introduction

Photovoltaic (PV) single-axis trackers rotate east to west about a horizontal north-south aligned axis to follow the sun. The basic design of a one-in-portrait tracker is shown in figure 1. This study focuses on the omega cold-formed steel mounting rail in figure 2, one of the most critical structural components [1]. The omega-type mounting rail is commonly used in commercial tracker designs from various suppliers. The rail is connected to the torque tube at mid-span and bolted to the PV modules at each end. Design trends in the industry show a decrease in the length of mounting rails to reduce the capital cost of utility-scale installations. This work investigates the influence of the rail length on displacement and stress distributions in the mounting rails and PV modules. The scope is limited to large-format bifacial modules, which show a growing market share for utility-scale tracker applications [2].

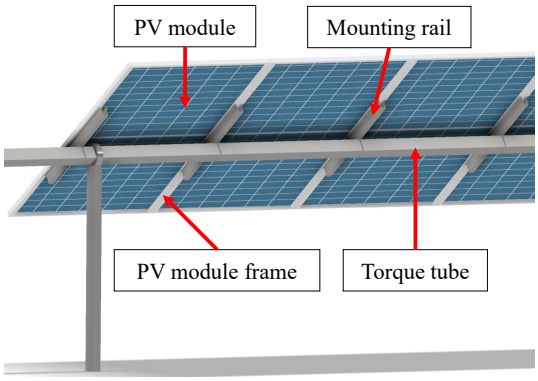

Figure 1 Single-axis tracker PV system.

According to benchmark cost models for PV systems [3], the PV modules are the largest cost component and account for 37 % of the total capital cost of a utility-scale (100 MW_{DC}) single-axis tracker plant without storage. When battery storage is added, the batteries account for the highest cost of 32 %, and the PV modules have the second highest cost at 20 %. The support structures, also called the structural balance of system (BOS), contribute 13 % and 8 % to these two different system designs. Considering the cost composition of a PV module itself, the crystalline silicon cells account for 40 % of the cost [4]. This high-level cost breakdown places the relative cost of PV modules, cells and structural components into perspective and emphasises the high cost of the modules.

Wind load considerations govern the structural design of

http://dx.doi.org/10.69694/2309-8988/2024/v40a6

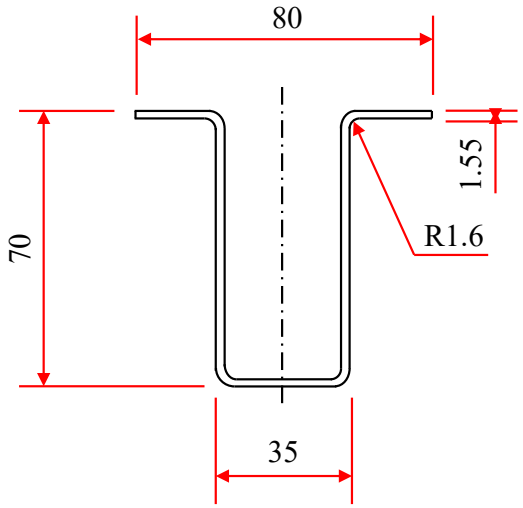

Figure 2 Mounting rail cross-section dimensions in mm.

large PV installations. Design codes such as ASCE 7-22 [5] can be used to determine statically equivalent wind loads to design the mounting rails and support structures. These design loads normally include an applied normal force and a moment about the torque tube axis. The mounting rails must adequately support the PV modules when subject to these wind load effects, which often have a high degree of associated uncertainty. Significant damage of single-axis trackers due to wind actions has been reported in literature [6], [7].

The current study is limited to simplified equivalent static wind loads. Actual aerodynamic wind loads are transient and unsteady due to atmospheric turbulence, buffeting and flow separation at the leading edges of inclined PV modules. Fatigue in mounting rails using load histories from full-scale field measurements was investigated by the authors in previous research [8]. The current study's findings may be useful in the preliminary design phase of new projects or the design of retrofitted mounting rails for plants that have suffered wind damage.

The PV modules are certified using the IEC 61215 qualification test standard [9]. These tests qualify the module design against common failure modes seen in previous designs but do not quantify reliability or life expectancy. Dynamic wind load testing applies 1000 cycles of a uniform 1000 Pa pressure load (but no moment) to the surface of the PV module while it is rigidly supported using the standard mounting holes on the PV modules. The rail length L_R refers to the longitudinal pitch length between these mounting holes. Shorter rails may not provide adequate support to the PV modules and could reduce the reliability of the installation. This study considered rail lengths of 900 mm, 790 mm, 600 mm, and 400 mm.

Crystalline silicon solar cells are brittle, thin (100 μm to 300 μm) and include surface imperfections and residual stresses resulting from manufacturing, making them prone to cracking [4]. The formation of cracks (width>30 μm) and micro-cracks (width<30 μm) can be attributed to manufacturing processes (ingot sawing, firing, soldering and lamination) and mechanical loads resulting from transportation, handling, installation and environmental conditions, specifically snow, wind and hail. Wind loads have been identified as one of the most common causes of cell damage. Reviewed literature shows that crack formation and propagation lead to decreased efficiencies and an overall reduction in reliability. Although a detailed investigation of cell fracture is beyond the scope of this work, the simulated correlation between peak tensile stresses and mounting rail length is presented. An increase in peak tensile stress would indicate an increased risk of cell cracking and related performance degradation.

2 Methodology

All analyses were conducted relative to the performance of a 900 mm reference rail. Resolving accurate absolute stresses would require implementing non-linear finite element (FE) models incorporating both geometric and material non-linearities, which is beyond the scope of this study. Residual stresses from the manufacturing process would also have to be accounted for.

2.1 Finite Element Models

A linear FE model was constructed for each rail length. Each model consisted of two PV modules (each measuring 2037 mm long and 1005 mm wide [10]) and three mounting rails, as seen in figures 3 and 4.

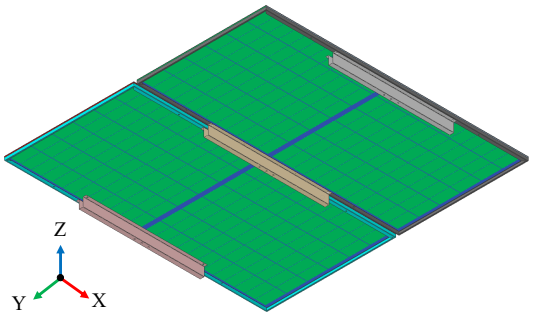

Figure 3 Bottom view of the FE model for $L_R = 900$ mm.

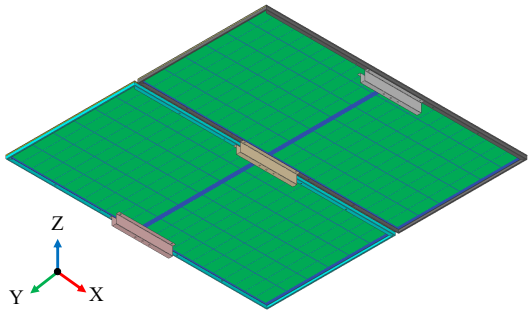

Figure 4 Bottom view of the FE model for $L_R = 400$ mm.

The PV modules used in this study consist of a glass laminate bonded to an aluminium frame. The glass laminate has five layers: glass, encapsulant, crystalline silicon solar cells, another encapsulant layer, and another glass layer. These layers were represented as an offset linear shell element mesh with nodes shared between layers. The frame consisted of aluminium box section extrusions 21 mm × 6 mm × 1 mm (height, width, thickness) with an additional 22 mm wide bottom flange. Glued contact was defined between the frame and glass laminate. Bolted connections between the module frames and rails are modelled using rigid multi-point con-

http://dx.doi.org/10.69694/2309-8988/2024/v40a6

straints with dependent nodes located on the edges of the bolt holes in both components. Non-linear contact and friction were not implemented to ensure the models retain their linear nature. Additional information about the geometry and FE models is available in [11]. Assessment of the PV module laminate was limited to the glass and the silicon cells. Comparisons for these components were based on principal stresses since these laminate components show brittle material behaviour. Linear elastic material properties in table 1 and small displacements were assumed to quantify relative changes in stress and displacement.

Table 1 Material properties used in FE simulations [12], [13],[13],[14],[15].

Material	Young's modulus [GPa]	Poisson's ratio [-]	Thickness [mm]
PV module glass laminate			
Solar glass (top)	70	0.20	2.0
Encapsulant uncal.	0.04	0.40	0.4
Encapsulant cal.	0.04	0.40	0.9
Crystalline silicon	166	0.28	0.2
Encapsulant uncal.	0.04	0.40	0.4
Encapsulant cal.	0.04	0.40	0.9
Solar glass (bottom)	70	0.20	2.0
PV module frame and mounting rail			
Aluminium	71.7	0.33	1.0 - 3.0
Steel	207	0.29	1.55

Translational constraints were applied to the connection between the mounting rails and the torque tube. Two simplified load cases representing wind loads were applied as pressure loads to the top surface of the PV modules. The first load case is a uniform unit pressure load of 1 kPa, similar to dynamic wind load testing in IEC 61215. The centre of pressure acts through the axis of the torque tube with zero eccentricity. The second load case is a linearly varying pressure load from 0 kPa at one end of the PV module to 2 kPa at the opposite end with an eccentricity of 340 mm. A moment is thus applied about the torque tube axis, which is more representative of code-based equivalent static wind loads. These loads were determined through extensive experimental testing on representative model-scale geometries in atmospheric boundary layer wind tunnels (refer to the commentary in [5]). Such studies have shown that aerodynamic loads acting on high aspect ratio inclined flat plate geometries have an eccentric centre of pressure, causing a net normal force and moment about the centre of the plate. The same trends have also been observed in field measurements [8]. The preprocessor used for this study was MSC Apex 2021 [16], and the solver was Genesis 18.0 [17].

The advantage of using linear FE models is that linear superposition can be used to calculate simulation results for site-specific wind loads consisting of a combination of normal forces and moments. This can be done as a post-processing step without requiring any further analysis. Results for different rail lengths can be compared efficiently for preliminary design purposes. Furthermore, this simplification is deemed acceptable for this study, which investigates the influence of rail length relative to a reference geometry in which L_R=900 mm.

2.2 Calibration of the FE Model

Uncertainties in the PV module material properties and geometry may introduce inaccuracies in the results. Thus, the FE models were calibrated using experimental force-displacement testing by adjusting the thickness of the encapsulant (and thus the overall thickness of the laminate). Thicker encapsulant layers place the two glass layers further apart, thereby increasing the area-moment of inertia (and stiffness) of the laminate. Figure 5 shows the setup used to apply a load to a well-defined area in the centre of the PV module. The module was simply supported using the standard mounting locations. Displacements were measured at several points on the PV module and compared to the FE model in figure 6. Within the range of loads used in this study, the load-displacement relationship was near-linear. However, this relationship is expected to become non-linear at higher loads due to large displacements and geometrical stiffness effects. The calibrated FE model shows a maximum deviation of 7 % compared to the measured displacement. The laminate layer thickness in table 1 lists the uncalibrated and calibrated encapsulant thicknesses. Although the overall laminate thickness was increased by 2×(0.9 mm-0.4 mm)=1 mm from the initial value obtained from the literature, it remained within 0.2 mm of the thickness measured at multiple points along the edge of the PV module.

Iterative analyses were performed to reduce the error between the simulation results and the experimental data, thereby calibrating the bending stiffness of the glass laminate. The calibration process considers a distributed load acting only on a portion of the laminate located in the centre of the laminate. This load simplification was necessary due to the challenging practical application of a uniform distributed load over a large surface. However, the partially distributed load causes out-of-plane bending deformation of the laminate, closely approximating the deformation expected for the simulated simplified wind loads that act over the full laminate surface.

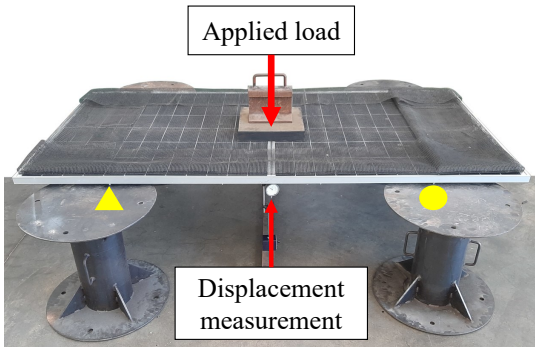

Figure 5 Calibration testing setup.

An alternative simplified calibration approach was investigated whereby a single glass layer with an adjusted Young's modulus was used to obtain comparable deformations. A single 4 mm glass layer (the total glass thickness) showed deformations up to 93 % higher than the measured values. Using a Young's modulus of 187 GPa leads to displacements within 1 % of the measured value at an applied load of 196 N. A 6 mm glass layer (the total laminate thickness) had 13 % lower displacements than the measured values. A calibrated Young's

http://dx.doi.org/10.69694/2309-8988/2024/v40a6

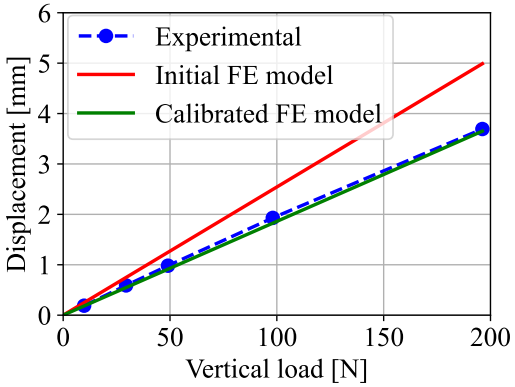

Figure 6 Measured and FE model displacements at the centre of the PV module.

modulus of 56.5 GPa leads to displacements within 1 % of the measured value. Using the total laminate thickness was thus a closer approximation to the full laminate. Although this method cannot calculate cell stresses, it may prove useful in the design and analysis of structural tracker components by using a model with reduced model complexity. In such simulations, the PV modules only need to have representative stiffness.

Most of the stiffness in the PV module is provided by the aluminium frame and glass. These materials are commonly used engineering materials that are well-characterised. Material properties from reputable sources were used, and model geometries were based on dimensional measurements. Results from the uncalibrated FE model were of the expected order of magnitude and confirmed that there were no major errors in the modelling approach. The calibrated laminate thickness deviated 3 % from the measured thickness. Furthermore, the calibrated Young's modulus in the simplified glass model (6 mm thick) was within 19 % of the nominal value obtained from literature and therefore deemed realistic.

3 Results

3.1 Displacement

Figures 7 and 8 show top and side views of the displacement of the longest and shortest rails when subjected to the two load cases. Tables 2 and 3 summarise the displacement results and compare relative changes in displacement for all assessed rail lengths. In these tables, the percentage change (indicated in brackets) is displacement relative to the 900 mm rail. The displacement component refers to the out-of-plane Z-component.

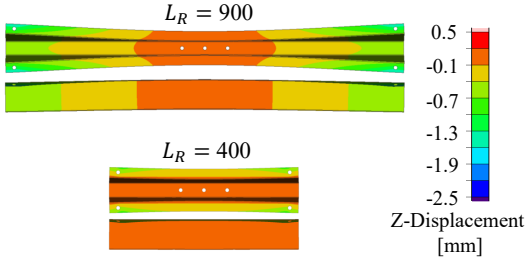

Figure 7 Rail displacement results for load case 1 (1 kPa uniform pressure).

The longer rails show larger deformation due to the global

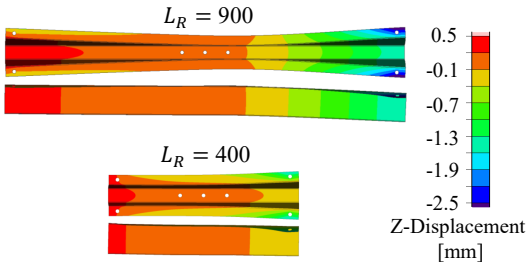

Figure 8 Rail displacement results for load case 2 (0 to 2 kPa distributed pressure).

Table 2 Maximum displacement results in the PV module and mounting rails for load case 1 (1 kPa uniform pressure).

Component	Load case 1, absolute [mm] (relative % change)			
L_R [mm]	900	790	600	400
Mounting rail (Z-comp)	-1.56 (-)	-1.24 (-21)	-0.89 (-43)	-0.81 (-48)
Mounting rail (Y-comp)	1.73 (-)	1.55 (-10)	1.26 (-27)	1.17 (-32)
Module frame (Z-comp)	-11.0 (-)	-13.3 (21)	-18.1 (65)	-24.4 (122)
Module laminate (Z-comp)	-11.0 (-)	-13.3 (21)	-18.1 (65)	-24.4 (122)

Table 3 Maximum displacement results in the PV module and mounting rails for load case 2 (0 to 2 kPa distributed pressure).

Component	Load case 2, absolute [mm] (relative % change)			
L_R [mm]	900	790	600	400
Mounting rail (Z-comp)	-2.78 (-)	-2.28 (-18)	-1.74 (-37)	-1.63 (41)
Mounting rail (Y-comp)	1.85 (-)	1.70 (-8)	1.50 (-19)	1.58 (-15)
Module frame (Z-comp)	-22.7 (-)	-27.0 (19)	-36.7 (62)	-52.7 (132)
Module laminate (Z-comp)	-22.7 (-)	-27.0 (19)	-36.7 (62)	-52.7 (132)

http://dx.doi.org/10.69694/2309-8988/2024/v40a6

bending of the rail. Local bending of the flanges at the bolted connections to the PV module is similar between the two rail lengths. Figures 9 and 10 compare the displacement of the PV modules. The dashed lines indicate symmetry planes between the two PV modules in the FE model. All displacement shapes are a combination of out-of-plane bending of the laminate due to the applied load, and bending of the PV module frame where it is not supported by the mounting rail. The non-uniform load case 2 causes substantially higher deformation compared to the uniform load case 1. A significantly higher displacement is observed with a decrease in rail length. A larger bending component of the PV module frame becomes dominant at shorter rail lengths where there is less support from the rail. The eccentricity of the equivalent normal force is 340 mm for load case 2. The PV module thus acts as a cantilevered beam for rails shorter than 680 mm. It is shown that deformations in the PV module frame and laminate can increase by as much as 132 % with a decrease in rail length.

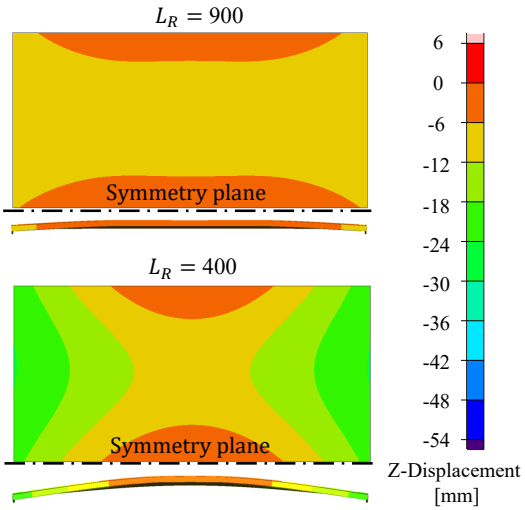

Figure 9 PV module displacement results for load case 1 (1 kPa uniform pressure).

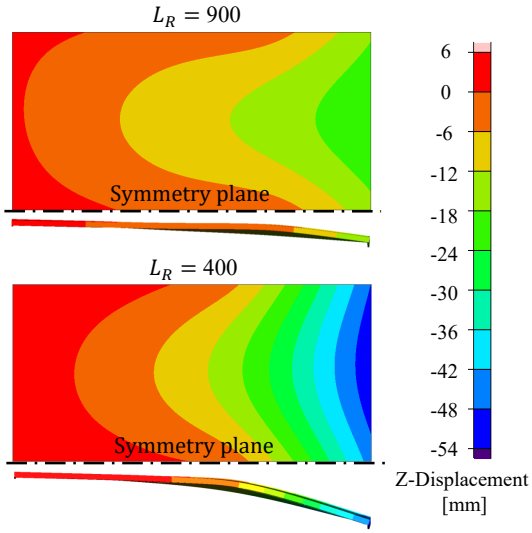

Figure 10 PV module displacement results for load case 2 (0 to 2 kPa distributed pressure).

3.2 Stress in Modelled Components

Stress in the mounting rail and PV module frame are assessed at fixed positions away from large stress concentrations. These positions are identified in figure 11, which shows a top view of a section of the PV module frame, and the top and side views of the 900 mm mounting rail. A fringe scale added to the figure shows Von Mises stress due to load case 2. Position 1 is located 120 mm away from the centre of the rail on the mid-plane of the bottom flange. Position 2 is 80 mm away from the centre of the rail on the top flange. Position 3 is 15 mm away from the bolted connection to the PV module frame. Positions 4 and 5 are located on the PV module frame and are 50 mm and 12 mm away from the bolted connection to the rail, respectively. Positions 1, 2, and 4 are expected to show only the effects of global bending. Positions 3 and 5 exclude the stress concentration effects from the bolt holes but include local bending effects.

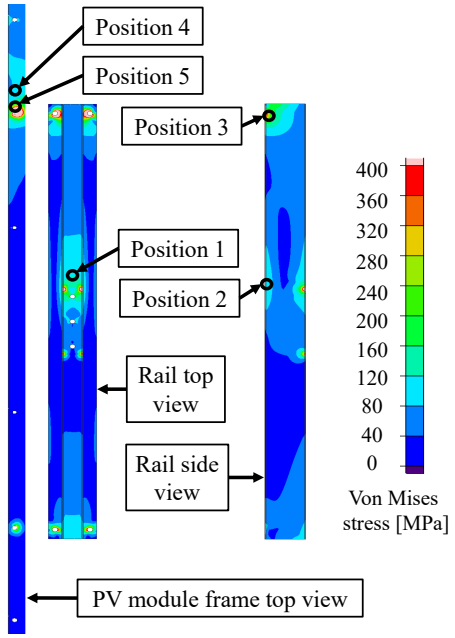

Figure 11 Positions used to assess stress in the mounting rail and PV module frame.

Tables 4 and 5 list the maximum Von Mises stresses at positions 1 to 5 in figure 11, for the various considered rail lengths. The peak maximum principal stresses in the glass and solar cells are also summarised. The relative change in stresses is given in brackets, with L_R=900 mm defined as the reference configuration. The stress in the mounting rail may increase or decrease with a reduction in rail length. Shorter rail lengths generate a smaller bending moment at the centre of the rail, and thus lower stresses at positions 1 and 2. However, the most critical position in the rails (position 3) showed a large increase in stress for load case 2. Position 3 experiences local bending of the mounting rail flange. Shorter rail lengths lead to a higher proportion of the equivalent load at the bolted connections transferred to one side of the mounting rail, and thus a larger bending stress. Positions 4 and 5 on the PV module frame showed substantial increases in stress with a reduction in rail length. Shorter rail lengths increase the unsupported length of the PV module. This increases the bending

http://dx.doi.org/10.69694/2309-8988/2024/v40a6

moment resisted by the PV module frame and thus leads to larger stresses. The maximum principal stresses in the glass and cells also increased significantly with a reduction in rail length.

Table 4 Maximum stress results in the PV module and mounting rails for load case 1 (1 kPa uniform pressure).

Comp./Pos.	Load case 1, absolute [MPa] (relative % change)			
L_R [mm]	900	790	600	400
Von Mises stress, σ_{VM}				
Position 1	54	46	39	41
	(-)	(-14)	(-27)	(-24)
Position 2	46	29	9.8	35
	(-)	(-36)	(-79)	(-23)
Position 3	218	222	229	236
	(-)	(2)	(5)	(8)
Position 4	52	65	89	117
	(-)	(25)	(70)	(124)
Position 5	208	225	270	269
	(-)	(8)	(30)	(29)
Maximum principal stress, σ_1				
Glass	19	21	24	28
	(-)	(8)	(26)	(43)
Cells	13	13	15	17
	(-)	(5)	(15)	(32)

Table 5 Maximum stress results in the PV module and mounting rails for load case 2 (0 to 2 kPa distributed pressure).

Comp./Pos.	Load case 2, absolute [MPa] (relative % change)			
L_R [mm]	900	790	600	400
Von Mises stress, σ_{VM}				
Position 1	101	90	75	80
	(-)	(-10)	(-26)	(-20)
Position 2	110	92	57	31
	(-)	(-17)	(-48)	(-72)
Position 3	390	414	476	607
	(-)	(6)	(22)	(56)
Position 4	90	110	147	188
	(-)	(22)	(62)	(108)
Position 5	334	374	480	532
	(-)	(12)	(44)	(59)
Maximum principal stress, σ_1				
Glass	34	38	44	57
	(-)	(10)	(29)	(65)
Cells	23	25	30	38
	(-)	(8)	(29)	(65)

The eccentric load case 2 resulted in a worst-case increase in stress and displacement of more than 100 % compared to load case 1. Load case 2 is thus the critical load case, even though only load case 1 is used to qualify PV modules against dynamic wind loads in IEC 61215. The inadequacy of using uniform pressure loading for dynamic load qualification testing has also been raised by other researchers [18].

The stresses in the mounting rails are compared in figures 12 and 13 for the different mounting rail lengths. Figures 14 and 15 show the top view of a section of the PV module frame. It can be seen that the size and magnitude of stress concentrations at the bolted connections generally increase with a reduction in rail length. Additionally, the highly stressed areas of the mounting rail and PV module frame increase in size for shorter rail lengths.

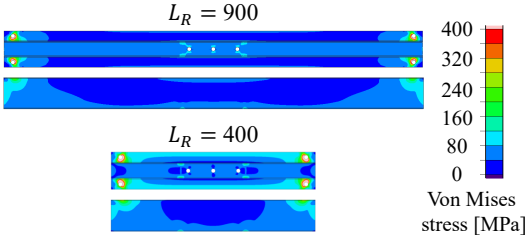

Figure 12 Rail stress results for load case 1 (1 kPa uniform pressure).

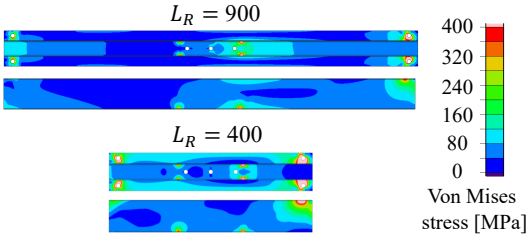

Figure 13 Rail stress results for load case 2 (0 to 2 kPa distributed pressure).

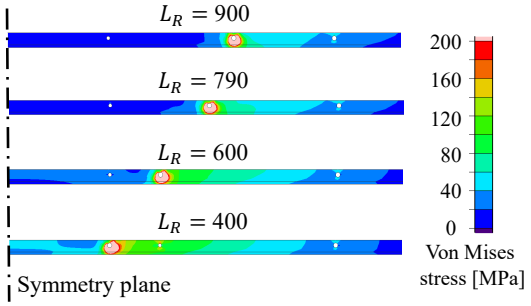

Figure 14 PV module frame stress results for load case 1 (1 kPa uniform pressure).

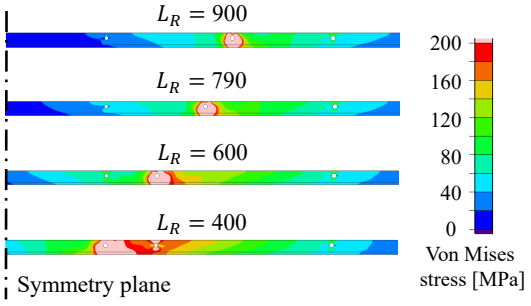

Figure 15 PV module frame stress results for load case 2 (0 to 2 kPa distributed pressure).

The glass showed an increase in maximum principal stresses with a reduction in rail length, as seen in figures 16 and 17. Similar behaviour was seen for the cells. The observed non-linear increase in stress is likely due to the combination of bending in the laminate due to the applied pressure load and bending of the PV module frame at the rail con-

http://dx.doi.org/10.69694/2309-8988/2024/v40a6

nections. The laminate bending component does not reduce, since the applied pressure is kept constant. Even though the PV module frame interacts with the mounting rails, the highest principal stresses in both the glass and cells were observed close to the locations of the rail attachments. A similar observation was made by [19].

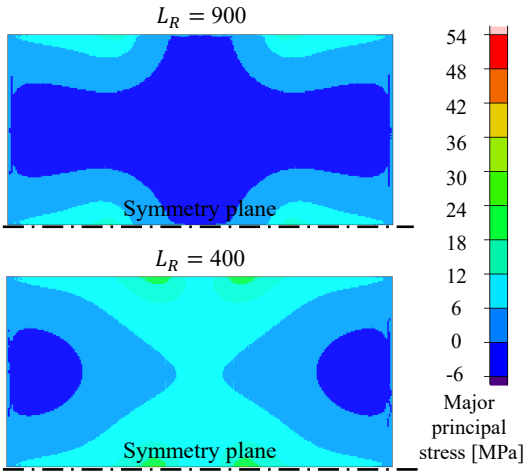

Figure 16 PV module glass stress results for load case 1 (1 kPa uniform pressure)

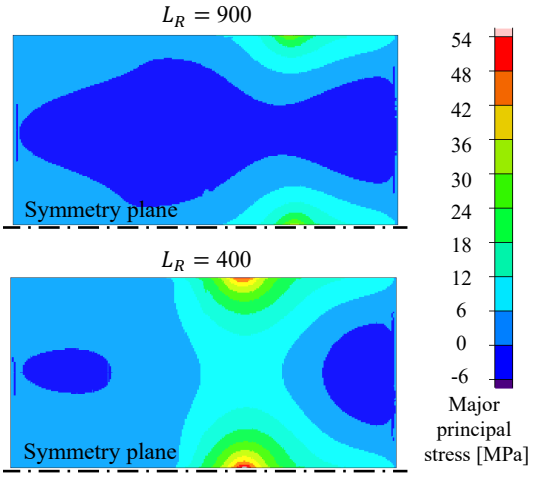

Figure 17 PV module glass stress results for load case 2 (0 to 2 kPa distributed pressure).

4 Conclusion

While cost savings may be realised by reducing the mounting rail length of utility-scale single-axis trackers, this may have a detrimental effect on the reliability of the PV modules.

1. Finite element models of PV modules may require calibration to match the measured displacement. Larger parts of the tracker could be simulated using a simplified approach with a single glass layer. Using the full laminate thickness of 6 mm required a Young's modulus adjusted to 56.5 GPa from the nominal value of 70 GPa.
2. While displacement of the rails reduce with a decreased rail length, the PV module displacement increased substantially. This is likely due to the reduction in the length of the PV module supported by the rails, leading to increased bending deformation of the modules. The decrease in rail length is associated with a significant reduction in the out-of-plane bending stiffness of the PV module and rail assembly. In general, a reduction in stiffness is expected to lead to an increase in the dynamic or resonant component of the wind loads.
3. Simplified wind loads in the form of uniform and non-uniform (linear varying) distributed loads were considered. Significantly higher stresses were seen from non-uniform loads with a centre of pressure eccentric to the torque tube, which more accurately represent wind loads according to structural design codes and field measurements. A uniform distributed load, typically used for dynamic load qualification testing on PV modules (IEC 61215), is not adequate to determine the required rail length to effectively resist wind loads. It is recommended to use representative eccentric loads for this purpose.
4. Shorter mounting rails lead to increased maximum stresses in the PV module and mounting rails. Far larger increases in stress were observed for the PV modules compared to the mounting rail. Eccentric loads showed larger increases in stress compared to uniform loads. Changing the rail length from 900 mm to 400 mm increases the peak Von Mises stresses in the module frame by up to 124 %. Maximum principal stresses in the both the solar glass and crystalline silicon cells increased by up to 65 %. The motivation for reducing rail length is to reduce tracker material cost. However, this potential cost saving must be carefully considered given the increased risk of mechanical damage to the high-cost PV modules and related performance degradation.

Acknowledgements

The authors would like to thank Scatec Africa for the use of an experimental PV plant, donation of several bifacial PV modules for testing purposes, and funding of the main author's studies.

References

[1] A. R. Wittwer, J. M. Podestá, H. G. Castro, J. L. Mroginski, J. O. Marighetti, M. E. De Bortoli, R. R. Paz, and F. Mateo. Wind loading and its effects on photovoltaic modules: an experimental–computational study to assess the stress on structures. *Solar Energy*, 240: 315–328, 2022.

[2] G. Masson and I. Kaizuka. *Trends in Photovoltaic Applications 2022*. International Energy Agency, 2022.

[3] V. Ramasamy, D. Feldman, J. Desai, and R. Margolis. U.s. solar photovoltaic system and energy storage cost benchmarks: Q1 2021. Technical report, National Renewable Energy Laboratory, November 2021.

[4] L. Papargyri, M. Theristis, B. Kubicek, T. Krametz, C. Mayr, P. Papanastasiou, and G. E. Georghiou. Modelling and experimental investigations of microcracks in crystalline silicon photovoltaics: A review. *Renewable Energy*, 145:2387–2408, 2020.

http://dx.doi.org/10.69694/2309-8988/2024/v40a6

[5] American Society of Civil Engineers. *ASCE 7: Minimum design loads and associated criteria for buildings and other structures*. American Society of Civil Engineers, Reston, VA, 2022.

[6] D. Valentín, C. Valero, and A. Egusquiza, M. Presas. Failure investigation of a solar tracker due to wind-induced torsional galloping. *Engineering Failure Analysis*, 135, 2022.

[7] P. Sanchez Molina. *Tracker failure in Spain*. PV Magazine, 2022.

[8] J. H Koekemoer, J. R. Bredell, G. Venter, and J. Reinecke. Field measurements of wind load effects in a photovoltaic single-axis tracker mounting rail. *Journal of Wind Engineering and Industrial Aerodynamics*, 253: 105876, 2024.

[9] International Electrotechnical Commission. *IEC 61215-1:2021 Terrestrial Photovoltaic (PV) Modules Design Qualification and Type Approval*. International Electrotechnical Commission, 2021.

[10] JA Solar. JAM72D10 400-420/MB datasheet, 2022. URL `https://www.jasolar.com`.

[11] J. H. Koekemoer. Dynamic wind load effects in a photovoltaic single-axis tracker mounting rail. Master's thesis, Mechanical and Mechatronic Engineering Department, Stellenbosch University, South Africa, 2024.

[12] f | solar. f | solarfloat, 2013. URL `http://www.fsolar.de/`. Solar glass datasheet.

[13] U. Eitner. *Thermomechanics of Photovoltaic Modules*. PhD thesis, Martin-Luther-Universität Halle-Wittenberg, Halle, 2011.

[14] L. Zhao, A. Maynadier, and D. Nelias. Stiffness and fracture analysis of photovoltaic grade silicon plates. *International Journal of Solids and Structures*, 97:355–369, 2016.

[15] R. G. Budynas and J. K. Nisbett. *Shigley's Mechanical Engineering Design*. McGraw-Hill Education, New York, 10 edition, 2015.

[16] Hexagon AB. *MSC Apex 2021, Nexus Portal*.

[17] Vanderplaats Research & Development. *Genesis Analysis Manual, Version 18.0*.

[18] S. Dietrich, U. Zeller, M. Pander, and M. Ebert. Evaluation of non-uniform mechanical loads on solar modules. In *Proceedings: IEEE 39th Photovoltaic Specialists Conference (PVSC)*, Tampa, Florida, 2013.

[19] Y. Lee and A. A. O. Tay. Finite element thermal analysis of a solar photovoltaic module. *Energy Procedia*, 15: 413–420, 2012.

http://dx.doi.org/10.69694/2309-8988/2024/v40a6
http://www.saimeche.org.za (open access)